Journal of Materials Chemistry

Cite this: *J. Mater. Chem.*, 2011, **21**, 11815

www.rsc.org/materials

PAPER

Sorting out semiconducting single-walled carbon nanotube arrays by preferential destruction of metallic tubes using water†

Pan Li and Jin Zhang*

Received 26th January 2011, Accepted 26th May 2011
DOI: 10.1039/c1jm10399g

The coexistence of metallic (*m*-) and semiconducting (*s*-) single-walled carbon nanotubes (SWNTs) in grown samples remains an obstacle in the application of SWNTs in nano-electronics. We report herein a rational approach to prepare well-aligned *s*-SWNTs using water vapor as a weak oxidant to etch the *m*-SWNTs during or after SWNTs growth. Water vapor with controlled concentration is carried into the furnace by argon gas during or after the SWNTs growth. It is found that the oxidation temperature and the concentration of water have a clear effect on the destruction of *m*-SWNTs. During SWNT growth (temperature above 800 °C), the introduction of water at a certain concentration only etches the SWNTs with small diameters and shows no selectivity between *m*-SWNTs and *s*-SWNTs. After SWNT growth, the water can etch *m*-SWNTs effectively with optimized oxidation temperatures and water concentrations. Micro-Raman spectra and electrical transport characterization confirm the selective etching effects. The mechanism of the selective etching of SWNTs with water is discussed based on the electronic structures of SWNTs. Using this method, densely packed and well aligned semiconductor SWNT arrays can be obtained. We believe this selective etching approach would largely broaden the application of SWNTs, especially for future nano-electronic and molecular detection devices.

Introduction

The excellent properties of single-walled carbon nanotubes (SWNTs) such as high mobility,[1] high current-carrying capacities,[2] and good stability[3] have inspired much research in potential applications. However, a bottle-neck in the application of SWNT, especially in nanoelectronics, is that almost all of the current available technologies are only able to produce a mixture of metallic (*m*-) and semiconducting (*s*-) SWNTs, which largely decreases the device performance. Many post-synthetic separation methods have been developed to separate *s*-SWNTs and *m*-SWNTs, such as electrophoresis,[4] physicochemical modification,[5] electrical breakdown,[6] ultracentrifugation,[7] chromatography[8] or agarose gel,[9] *etc.*[10,11] All these approaches can effectively separate semiconducting tubes with a very high percentage. However, since almost all these separation methods are solution-based, SWNTs are usually in a random formation, and very importantly, they are chemically decorated. This has the effect of largely changing the surface chemistry of the tubes or even the electronic structure and properties of the tubes.

Recently, *in situ* selective growth has become an alternative methodology for sorting semiconducting or metallic SWNTs without chemical decoration. By selecting suitable carbon sources,[12] *in situ* ultraviolet (UV) irradiation,[13] or changing thermal annealing ambient of the catalyst particles,[14] *s*-SWNTs or *m*-SWNTs can be obtained. These methods are still barely satisfactory due to the poor selectivity in *in situ* growth. It seems powerless to selectively grow (10, 10) *m*-SWNTs or (9, 11) *s*-SWNTs with a diameter difference of only 0.03 Å by controlling the catalyst particle. Meanwhile, the selective growth mechanism is still not clear for the existing *in situ* selective growth approaches. Developing more methods with clear mechanisms for the selective growth to get high separation efficiency is highly desirable for practical applications.

In fact, since the first report that *m*-SWNTs can be selectively functionalized by chemicals,[15] covalent sidewall functionalization strategies have been widely used to separate *m*- and *s*-SWNTs in solution-phase[16] and gas-phase.[11,17] During the separation process, *m*-SWNTs were selectively removed due to the abundance of electron density near the Fermi level. Among all these strategies, gas-phase oxidization introduces less

Center for Nanochemistry, Beijing National Laboratory for Molecular Sciences, Key Laboratory for the Physics and Chemistry of Nanodevices, State Key Laboratory for Structural Chemistry of Unstable and Stable Species, College of Chemistry and Molecular Engineering, Peking University, Beijing, 100871, P.R. China. E-mail: jinzhang@pku.edu.cn; Fax: +86-10-6275-7157; Tel: +86-10-6275-7157

† Electronic supplementary information (ESI) available: Typical Raman spectra of SWNTs grown with 2000 ppm water introduced, AFM images of SWNT grown with and without 1000 ppm water introduced. Tabulated data of effects of temperature, water concentration and reaction time on the etching of SWNTs, statistics of the log (I_{ON}/I_{OFF}) of 30 single-tube FET devices which were etched by water (3000 ppm, 20 min, 720 °C), SEM images of the FET devices comprising large scale arrays, and other expanded discussions. See DOI: 10.1039/c1jm10399g

contamination, such as salts and surfactants (including DNA) into the system, therefore it has been widely used to minimize undesired chemical decoration to the *s*-SWNTs. Further, the gas-phase oxidation can also remove *m*-SWNTs without affecting the alignment of *s*-SWNTs arrays on a surface which is also critical for nano-electronic applications. However, the available gas-phase or liquid-phase selective chemooxidation approaches cannot remove all the *m*-SWNTs.[18] Most importantly, these approaches also introduced certain perturbation to the electronic structure and surface chemistry of the *s*-SWNTs due to the utilization of strong oxidants, such as H_2O_2,[19] O_2[17] and O_3.[20] Therefore choosing a suitable oxidizer is very important to achieve selective removal of *m*-SWNTs.

As a mild oxidizer, with moderate reactivity to oxidize carbon material, water has long been used for the purification of SWNTs in HIDE (hydrothermally initiated dynamic extraction) treatment.[21] It has also been used for cleaning amorphous carbon on the catalysts during growth of super dense vertically aligned nanotube forests.[22] Moreover, water is also a clean reagent as the products are mostly CO or CO_2, which introduce little contamination to the SWNTs. However, it has never been studied for selective etching of *m*-SWNTs.

In the present study, as shown in Fig. 1, well aligned *s*-SWNT arrays are obtained by selective removal of *m*-SWNTs with water based on the different electronic structures of *s*-SWNTs and *m*-SWNTs. Horizontally aligned SWNT arrays with high density were grown on single crystal stable temperature (ST)-cut quartz surface using ethanol as the carbon source. Water was introduced to the furnace during or after the growth to selectively remove *m*-SWNTs. When water was introduced during SWNTs growth (temperature above 800 °C), it is found that a large number of SWNTs with small diameters could be etched away with no selectivity for *m*-SWNTs or *s*-SWNTs. This might be because the high temperature (above 800 °C) applied for SWNT growth makes the thermal excitation comparable to the band-gap energy of the semiconducting SWNTs. As a consequence, the difference of semiconducting and metallic SWNTs toward reacting with water due to the different electronic structures becomes indistinct. When water was introduced after SWNT growth, selective etching away *m*-SWNTs could be achieved; however, the oxidation temperature and water concentration had significant effects. Experimental results by scanning electron microscopy (SEM), Raman spectroscopy, and electronic measurements of the SWNT arrays remaining on the substrate surfaces indicate that, under oxidation temperatures of 700–750 °C and a water concentration of 6000 ppm, *m*-SWNTs were selectively oxidized and the *s*-SWNTs were barely affected. Specifically, the statistics of single-tube field effect transistor (FET) behaviors of the remaining tubes suggested that the best separation yield of *s*-SWNTs could be close to 100%.

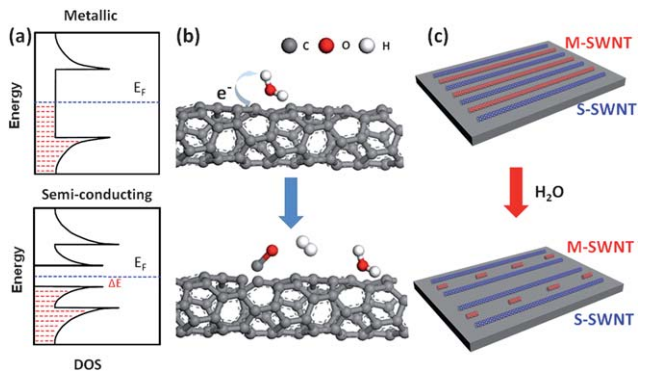

Fig. 1 Scheme of selective etching of *m*-SWNTs by water. (a) 1D density of states plots near Fermi level (E_F) for semiconducting SWNTs and metallic SWNTs. The reactivity is dependent on the availability of electrons near E_F; (b) water extracts electrons from the nanotubes, thus evolving H_2 and CO gas. The defect-contained nanotubes could further react with water; (c) water selectively etches *m*-SWNT and leaves *s*-SWNTs on the substrate. Blue, semiconducting SWNTs; Red, metallic SWNTs.

Experimental section

Growth of SWNT arrays

The substrates used were single-polished ST-cut quartz wafers (miscut angle <0.5°), which were bought from Hefei Kejing Technology Co., China. After cleaning, the quartz substrates were annealed at 900 °C in air for 8 h. 50 mM $CuCl_2$/ethanol solution, used as the catalyst solution, was patterned onto the quartz surface by "Needle-Scratching".[23] The substrate was then heated to 850 °C in air, and kept for 10 min in a gas flow of 100 sccm of argon and 100 sccm of hydrogen, followed by CVD growth of SWNTs at 850 °C for 40 min. A flow of 40 sccm of hydrogen together with 20 sccm of argon through an ethanol bubbler was used to synthesize the SWNT arrays. The as-grown SWNTs were inspected with scanning electron microscopy (SEM, Hitachi S4800 field emission, Japan), atomic force microscopy (AFM, Veeco NanoScope IIIA,Veeco Co.), and a Raman spectrometer (Horiba HR800 Raman system).

Water vapor introduction

Water was introduced by an argon flow through a water bubbler. The argon flow carrying the water vapor was diluted with another flow of argon. The water vapor concentration was adjusted by varying the flow rate of the argon bubbling water. The specific concentration was calculated assuming that the partial pressure of water vapor in argon flow is equivalent to the saturated vapor pressure of water at 20 °C (room temperature). The gas circuit connecting the water bubbler and the reactor (1 inch quartz tube) was designed to be short to make sure the water vapor mixed with all the other gases within 30 s to avoid inaccuracy caused by a delay.

Raman spectroscopy characterization

Resonant Raman spectroscopy (RRS) has been used to probe the detailed structure and the electronic properties of the SWNT arrays. The radical breathing mode (RBM) of the Raman spectra was used to distinguish semiconducting and metallic SWNTs. Resonant Raman spectroscopy was recorded using 633 nm and 514 nm lasers with laser spot size of ~1 μm. RRS characterization was carried out directly on the quartz substrate, and was also carried out by transferring the SWNT arrays onto SiO_2/Si substrates in order to avoid influences of the strong Raman signal from single-crystal quartz at 127 and 205 cm^{-1}. The

interspot spacing in the line-mapping mode was set as 0.8 μm to make sure sufficient Raman signals were collected in the mapping area.

Electrical measurement

After the SWNT arrays were transferred from quartz to SiO_2/Si substrate, back gate FETs were fabricated. The source and drain electrodes patterns were defined on the substrates by electron beam lithography (EBL). The source and drain electrodes were made by Cr (5 nm)/Au (50 nm). A Keithley 4200-SCS semiconductor characterization system with a probe station was used to do the transport measurement. The measurement was carried out in air at room temperature.

Results and discussion

Surface lattice guided growth of SWNTs by chemical vapor deposition (CVD) has proven itself a powerful method to obtain horizontally aligned SWNTs arrays on surfaces such as sapphire[24] and quartz.[25–27] Using the growth process described in the experimental section, well aligned SWNTs with a high density were grown on a ST-cut quartz surface. Fig. 2 shows the SEM, AFM images and Raman spectra of the typical as-grown SWNT arrays. The SEM image indicates that the well aligned SWNTs arrays with high density are uniform over a large area with length up to 300 μm. AFM characterization shows that the density of the highly aligned SWNTs are around ~4 tubes/μm and the diameters of the carbon nanotubes are below 2.3 nm, indicating that the arrays consist of purely SWNTs without much amorphous carbon contamination. Fig. 2c shows a typical Raman spectra of the SWNT arrays with 633 nm laser excitation after the arrays were transferred onto the SiO_2/Si substrate. Abundance of RBM with a wide distribution between 110 and 250 cm^{-1} confirms that the tubes arrays are a mixture of *m*-SWNTs and *s*-SWNTs.

Introducing water vapor to the furnace during SWNTs growth

All the synthesis conditions remained the same when water vapor was introduced. The flow rate of the argon that was used to dilute the water concentration was set at 100 sccm, and the flow rate of the argon bubbling the water was varied to tune the water concentration. Fig. 3a–c are SEM images of SWNTs grown with different concentrations of water vapor introduced. As shown in Fig. 3a, when water vapor with a concentration lower than 1000 ppm was introduced during the growth, the density of the

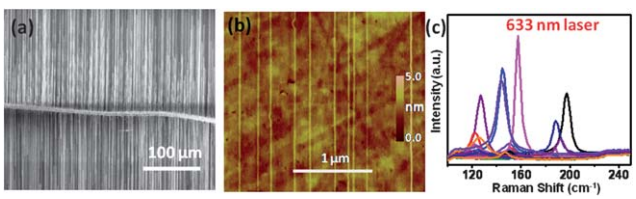

Fig. 2 (a) SEM image and (b) AFM tapping-mode topographic image of the well-aligned SWNT arrays on ST-cut quartz; (c) typical Raman spectra of the SWNT arrays transferred onto SiO_2/Si substrates (λ_{ex} = 633 nm).

SWNTs arrays was not affected compared with the results without any water introduction. However, with a water concentration higher than 2000 ppm, the density decreased significantly to ~1 SWNT/5 μm. When the water concentration continued to increase to 6000 ppm, only a few very short SWNTs were found on the surface. Regardless of the SWNTs array's density, all the SWNTs appear to be continuous and without discontinuous fragments.

The role of water in reducing the growth efficiency indicated that water reacted with the growing carbon nanotubes. Water directly reacting with the hydrocarbon source, a well-known phenomena called 'steam reforming' was excluded by the low water concentration used here.[28] As can be seen from Fig. 3, independent of the water vapor concentration, all the SWNT arrays were well aligned along the same direction, which implies that the lattice of the substrate was not destroyed by water at such high temperature. Therefore water etching the growing carbon nanotubes is considered to be the main reason for the observed decrease in the array density. Water concentration can exert a big influence on the etching effect. Empirically, water concentration of 100–200 ppm is known to maximize the synthesis efficiency in the super-growth of vertically aligned SWNT arrays,[28] but higher concentration levels will lower the synthesis efficiency. Hence, it is speculated that a relatively higher concentration of water, as used here, can indeed etch the carbon nanotubes.

To obtain a quantitative estimation of possible selective etching during SWNT growth, micro-Raman mapping was recorded over a large area of the SWNTs array by two excitation wavelengths of 633 nm and 514 nm. Fig. 3d shows the Raman spectra of SWNTs grown with 2000 ppm of water introduced. From over 40 nanotubes which had normal G-band signals with the two laser excitations, only three RBM peaks lower than 140 cm^{-1} were collected. Most of carbon nanotubes have a weak G-band (see Figure S1 in ESI†) but no obvious D-band, indicating that water doping of the carbon nanotubes might occur at such a high temperature.[29] In fact, the RBM signal of large diameter tubes (d >2 nm) is expected to be weak and hardly observable.[30] Therefore it was speculated that lack of RBM signals was caused by the enrichment of large diameter SWNTs through water etching the small diameter carbon nanotubes at this high temperature. Fig. 3e shows the AFM histogram of the diameter of SWNTs grown with no water (black) and 2000 ppm water (red) introduced. The SWNTs arrays grown with water had a significantly lower percentage of SWNTs with a diameter smaller than 1 nm, only 5%. Without water introduction, the percentage of small diameter SWNTs is 18%. The statistics of the tube diameter distribution confirmed that water etched the small diameter SWNT preferentially. It could be seen obviously from the inset AFM image that the SWNTs left on the substrate were clean and continuous, which implies a fast and complete reaction of water with SWNT and amorphous carbon. The results of the experiment designed to elucidate the etching effect of water to carbon is shown in Figure S2 in ESI.†

To further understand how water oxidation affects the electronic types of SWNT arrays, we measured the transport properties of SWNTs grown with (2000 ppm) and without introduced water. Both FETs contain equivalent nanotubes (~100 tubes) in the channel region. As shown in Fig. 3, the devices exhibited

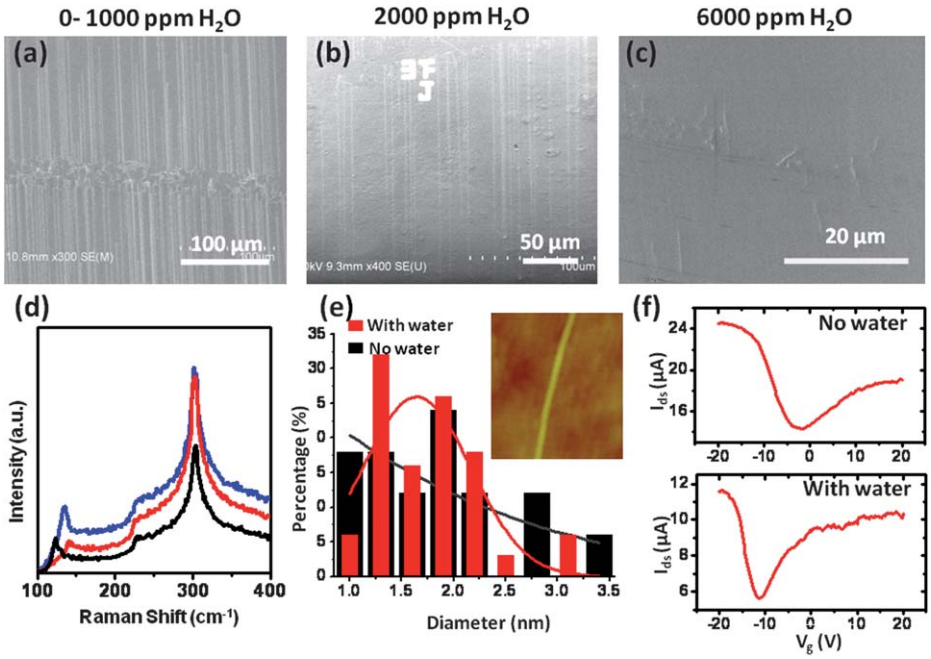

Fig. 3 (a–c) SEM images of SWNT arrays grown with different water concentration. (d) Micro-Raman spectra of SWNTs grown with 2000 ppm water introduced. Over 40 nanotubes which had normal G-band signals with the two laser excitations (633 nm and 514 nm), only three RBM peaks lower than 140 cm^{-1} were collected. (e) Diameter distribution of SWNTs grown with 2000 ppm water introduced and without water, and a typical AFM image of the SWNT grown with water introduced (insert). (f) Transfer characteristics of FET devices fabricated with the two kinds of samples under a bias voltage $V_{ds} = 100$ mV.

similar p-type transport behavior with on/off ratios less than ~2. This result indicates that the percentage of *m*-SWNT in the sample did not decrease remarkably by water etching during the growth. As described above, only diameter selectivity but not electronic property selectivity occurred when the water was introduced during the SWNTs growth. Therefore, introducing water after SWNTs growth was used to separate *m*-SWNTs and *s*-SWNTs.

Introducing water vapor to the furnace after SWNTs growth

Introducing water vapor after SWNT growth can give enough room for investigating the effect of oxidation time, oxidation temperature and concentration of water on selectively etching *m*-SWNTs. We varied the oxidation temperature from 950 to 500 °C. Other reaction conditions were changed including water concentration and reaction time. The typical results are listed in Figure S3 in ESI.† At temperatures higher than 800 °C, water etches all the SWNTs even with low concentration of water and a short reaction time. In contrast, at temperatures from 550 to 650 °C, water is less active and reacts with SWNTs mildly. As shown in Fig. 4a and 4b, introduction of 2000 ppm water at 650 °C to react with as-grown SWNTs on quartz substrate for 30 min led to obvious damage to some of the SWNTs but did not decrease the density very much.

The Raman mapping was set as ~1 μm laser spot size and 0.8 μm interpot spacing in order to make sure almost every single SWNT could be examined. The obtained results were compared before and after the etching process. The SWNTs synthesized in our system had a diameter distribution from 1.0 to 2.0 nm (determined by AFM), which means metallic SWNTs (E_M[11]) and semiconducting SWNTs (E_S[33]) are resonant in a nearly 50/50 ratio with a 1.96 eV line. Therefore a majority of the characterizations were performed with 632.8 nm (1.96 eV) excitation. The

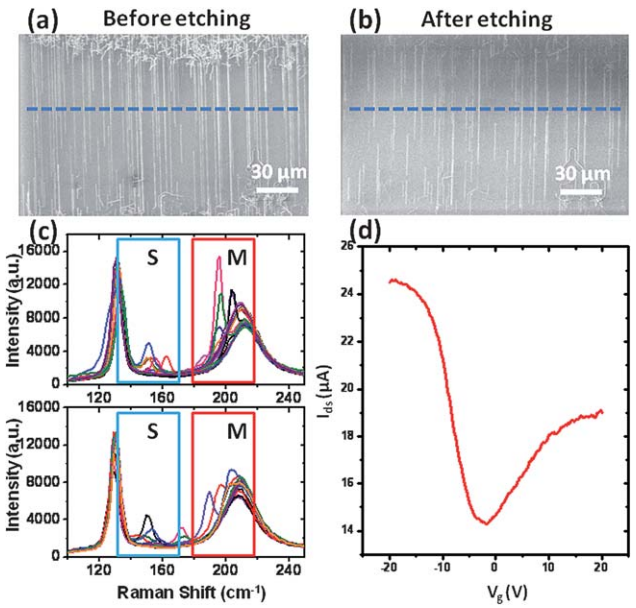

Fig. 4 Selective etching of *m*-SWNTs on quartz with 2000 ppm water. (a, b) SEM images of SWNT arrays on quartz before and after water etching; (c) Micro-Raman spectra of SWNTs on quartz at 633 nm excitation before (up) and after (down) water etching. Raman mapping line was marked with a blue dashed line in (a) and (b); (d) transfer characteristics of devices fabricated with the arrays after etching. The measurement was carried out under a bias voltage $V_{ds} = 100$mV.

Raman spectroscopy experiment was performed on quartz substrate before and after water was introduced. As shown in Fig. 4c, peaks in the region from 120 to 165 cm^{-1}, which are assigned to semiconducting tubes (E_S[33]), did not change very much under 633 nm laser excitation. However among peaks at the region from 170 to 240 cm^{-1}, which were assigned to metallic tubes (E_M[11]), 50% of them had disappeared and the remaining ones had a decreased intensity. Meanwhile, a transport property measurement was performed after the etched arrays were transferred onto the SiO_2/Si substrate. The transport curve of the FET device shown in Fig. 4d has an on/off ratio less than ~2. The above results suggest that the reaction conditions were not intense enough to totally remove all the metallic tubes.

To obtain a more complete separation result, we increased the oxidation temperature to create a stronger oxidative environment. The as-grown SWNT arrays were transferred to the SiO_2/Si substrate, and then Raman characterization was carried out before the etching process was performed. A temperature range of 700 to 750 °C was used, with a reaction time of 20 to 30 min and water a concentration of 2000–6000 ppm. Fig. 5a and 5b shows SEM images before and after reaction for 30 min with 6000 ppm water introduced at a velocity of 70 sccm at 700 °C. We found that the density of SWNT arrays decreases by ~35%. The AFM image of the SWNT arrays after etching in Fig. 5c shows that part of the array has been destroyed into fractions. Meanwhile some of the SWNTs remain unaffected along the whole tube, which indicates a selective reaction of water with the SWNT arrays. Raman line mapping results were shown in Fig. 5d–f. With 633 nm laser excitation, both metallic and semiconducting SWNTs were detected in large numbers in the pristine sample. 80% of *m*-SWNTs were etched away while more than 90% of *s*-SWNTs remained in the same mapping region (indicated as a blue dashed line in the SEM images), as shown in Fig. 5e. Combined with the additional Raman mapping with a 514 nm laser excitation shown in Fig. 5f over the region, we conclude that what remains in the SWNT arrays is mostly *s*-SWNTs. Furthermore, from Fig. 5d and 5e, we found that for SWNTs with a smaller diameter of 1.0–1.5 nm (calculated by the experimental formula $\omega = 248/d$[31]), most of the metallic SWNTs were removed. Nonetheless, as seen in Fig. 5f, considerable numbers of semiconducting SWNTs were still detected in this diameter range after the reaction. Thus the change in spectral characteristics was not induced by diameter selectivity but electronic type selectivity. In another case, we chose a special sample in which over 90% of the detected SWNTs were metallic nanotubes and only 2 SWNTs were semiconducting ones (the growth

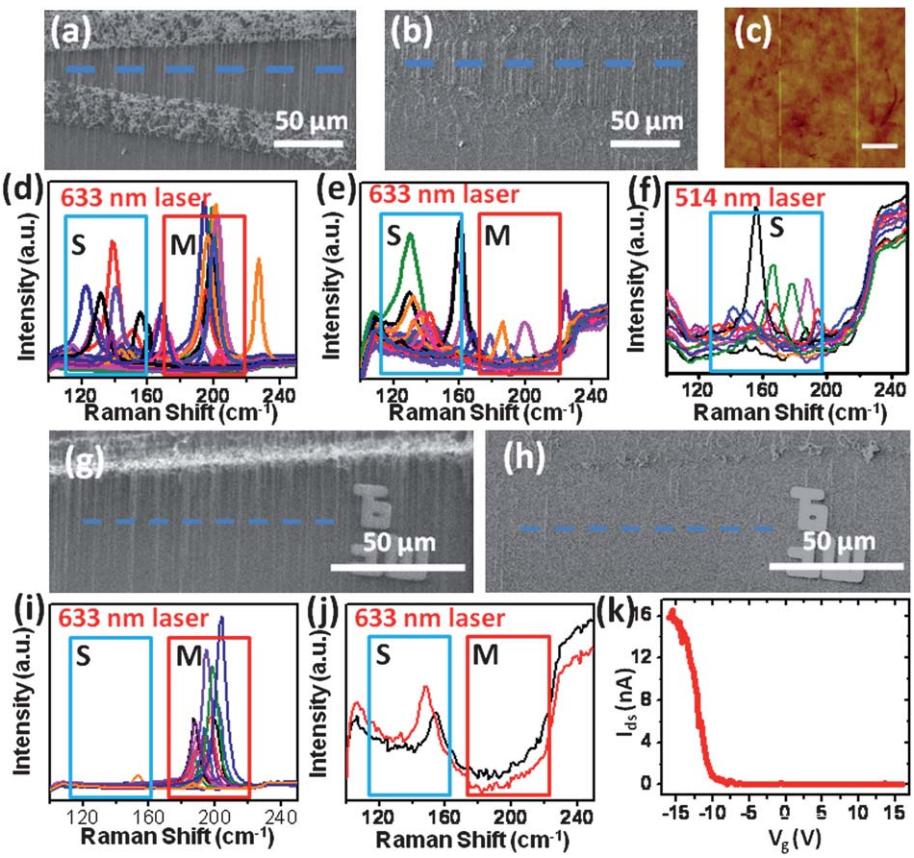

Fig. 5 Selective etching of *m*-SWNTs by water on SiO_2/Si substrate. The water concentration was 6000 ppm. (a, b) SEM images of SWNT arrays before and after water etching at 700 °C; (c) AFM image of the SWNT arrays after water etching at 700 °C, the scale bar is 500 nm; (d–f) Micro-Raman spectra of SWNTs at the excitation wavelength of 633 nm and 514 nm before (d) and after (e, f) water etching. Raman mapping line was marked with a blue dashed line in (a) and (b); (g, h) SEM images of SWNT arrays before and after water etching at 750 °C; (i, j) micro-Raman spectra of SWNTs before (i) and after (j) water etching. Raman mapping line was marked with a blue dashed line in (g) and (h); (k) transfer characteristics of one of the test devices fabricated with the arrays after etching under a bias voltage $V_{ds} = 10$mV.

method will be depicted elsewhere). A higher temperature of 750 °C and reaction time of 20 min were used with other conditions unchanged. As shown in Fig. 5h, few SWNTs were found left on the substrate in the SEM image. It is easily judged from the Raman spectra in Fig. 5i and 5j that 100% of the *m*-SWNTs were etched and *s*-SWNTs remained intact, in agreement with Fig. 5h.

Selective etching of *m*-SWNTs was also confirmed by transport property measurements. After the water oxidation process, FETs were fabricated with the remaining SWNT arrays on SiO_2/Si substrates. A typical FET with channel width of 500 μm and a channel length of 2 μm containing more than 400 SWNTs (see Figure S6 in ESI†) exhibited p-type behavior and was completely switched off at a threshold voltage of −8 V, as shown in Fig. 5k. The on/off ratio was about 3000 and the off current was in the picoamp range indicating *m*-SWNTs were totally removed. The relatively small output current may be caused by the low bias voltage of only 10mV, or the high percentage of semiconducting nanotubes in the array.[32] Electrical transport properties were also measured in single-tube FETs with a channel width of 10 μm and a channel length of 2 μm. The statistics of transport behavior of 30 devices shows that almost every carbon nanotube are *s*-SWNTs (see Figure S4 in ESI†).

Mechanism of selective etching of *m*-SWNTs by water

The driving force for water to preferentially react with *m*-SWNTs can be explained by thermodynamics. The reaction of water etching SWNTs can be described as follows:

$$C(s) + H_2O(g) \rightarrow CO(g) + H_2(g)$$

Density functional theory (DFT) calculations[33] show that per-unit-length formation energy is higher for *m*-SWNTs than *s*-SWNTs for a given value of diameter. It is reasonable to assume therefore that, for *s*- and *m*-SWNTs with similar diameters, the reactions with *m*-SWNTs have a higher enthalpy change, ΔH. Furthermore, assuming the entropy change of the reaction is the same, the difference in enthalpy change brings an equal quantity of change to ΔG (Gibbs free energy change). As a symbol of reaction favorability, a decrease of ΔG suggests a reaction is more reactant-favored. Take *m*- and *s*-SWNTs both with diameters of 1 nm as an example, the formation energy (ΔH_f) of a *m*-SWNT with length of 1.46 Å (C–C band length) is higher by ~0.15 eV than a *s*-SWNT with the same length. This is substantial because the standard equilibrium constant will be ~100 times higher. (Detailed calculation is illustrated in supporting information.†) Thus the preferential etching of *m*-SWNTs is feasible given this small but distinguishable difference.

Two factors are crucial to successfully sorting out *s*-SWNTs from the as-grown SWNT arrays by chemical reaction. One is the concentration of water vapor and the other is the temperature which is maintained during the reaction. Water assisted growth of both vertically aligned carbon nanotubes[22] and SWNT films[34] has been studied, and the related mechanism was investigated extensively.[35,36] The unique property of water that can be used to selectively etch amorphous carbon, but not the carbon nanotubes, during the growth makes it a promising candidate for the separation of metallic and semiconducting SWNTs. The effects of water vapor on diameter distribution of SWNTs were discovered and fully explored by Ago's group;[34] no electronic property selectivity but a narrow distribution of certain specific chirality was reported. It was supposed the different water concentrations could lead to different initial reaction rates with carbon materials, therefore a relatively low concentration may just etch the amorphous carbon and/or nanotubes of very small diameter but has little effect on the majority of the as-grown carbon nanotubes. According to our observation, a water concentration higher than 1000 ppm can make a difference toward reactions with SWNTs.

As usually known, the growth of horizontally aligned SWNT arrays often needs a high temperature, at which water may have lost its capability to differentiate metallic and semiconducting SWNTs through the etching reaction. This is because at high temperatures the oxidation capability of water has increased and the differences in electron density near E_F between *m*-SWNT and *s*-SWNT have blurred. The influence of temperature on the distribution of free carriers is reflected by the Boltzmann factor, which is termed as,

$$e^{-E_g/(kT)}$$

where E_g is the band gap energy (E_{11}) of a semiconducting SWNT, and k is the Boltzmann constant. Here, the Boltzmann factor gives the (unnormalised) relative probability of an electron in the conducting band being excited to the valence band due to thermal activation. The E_{11} varies from ~0.1 eV to ~1 eV depending on the diameter of the semiconducting SWNTs. When E_{11} adopts an energy of 0.5 eV, the value of the Boltzmann factor at 900 °C, a typical temperature for SWNT growth, is ~2 times higher than that at 750 °C. Considering the huge number of carriers in the SWNTs, this difference can make significant electrons in the conducting band of *s*-SWNTs excited to the valence band at high temperatures. It certainly means the *s*-SWNTs have much less difference from the *m*-SWNTs, therefore high growth temperature is a big hurdle to the separation of *s*- and *m*- SWNTs during growth. This is similar to our results: during the SWNTs growth, due to the high temperature, it only has diameter selectivity and no *m*- and *s*-SWNTs selectivity; After the growth, selective reaction based on electronic type could be achieved when 2000–6000 ppm water vapor was introduced at a relatively lower temperature of 700–750 °C. In fact, this diameter selectivity at high temperature also can be understood through mechanisms previously developed based on the carbon pyramidalization angle,[37,38] which means carbon nanotubes of different diameters have different reactivity because they have different strain energy of pyramidalization.

Conclusion

Horizontally aligned semiconducting SWNT arrays were obtained by selectively etching away the metallic SWNT populations with water vapor. We have achieved high separation efficiency. Extensive Raman and SEM studies demonstrated that water vapor concentration and the reaction temperature significantly influenced the etching selectivity. With optimized conditions, a FET containing 400 carbon nanotubes can be switched

off completely, indicating that the metallic tubes can be completely removed. The 'clean and quick' sorting method developed in this work can maintain the perfect alignment of the carbon nanotubes with good control of the electronic type uniformity, thus it can be considered to contribute an reliable solution to the major problems existing in the application and integration of carbon nanotubes in future nano-electronics.

Acknowledgements

This work was supported by NSFC (50972001, 20725307 and 50821061) and MOST (2011CB932601, 2007CB936203).

References

1 A. Javey, H. Kim, M. Brink, Q. Wang, A. Ural, J. Guo, P. McIntyre, P. McEuen, M. Lundstrom and H. J. Dai, *Nat. Mater.*, 2002, **1**, 241–246.
2 X. J. Zhou, J. Y. Park, S. M. Huang, J. Liu and P. L. McEuen, *Phys Rev Lett*, 2005, 95.
3 J. T. Hu, T. W. Odom and C. M. Lieber, *Acc. Chem. Res.*, 1999, **32**, 435–445.
4 R. Krupke, F. Hennrich, H. von Lohneysen and M. M. Kappes, *Science*, 2003, **301**, 344–347.
5 D. Chattopadhyay, L. Galeska and F. Papadimitrakopoulos, *J. Am. Chem. Soc.*, 2003, **125**, 3370–3375.
6 P. C. Collins, M. S. Arnold and P. Avouris, *Science*, 2001, **292**, 706–709.
7 M. S. Arnold, A. A. Green, J. F. Hulvat, S. I. Stupp and M. C. Hersam, *Nat. Nanotechnol.*, 2006, **1**, 60–65.
8 M. Zheng, A. Jagota, E. D. Semke, B. A. Diner, R. S. Mclean, S. R. Lustig, R. E. Richardson and N. G. Tassi, *Nat. Mater.*, 2003, **2**, 338–342.
9 T. Tanaka, H. Jin, Y. Miyata, S. Fujii, H. Suga, Y. Naitoh, T. Minari, T. Miyadera, K. Tsukagoshi and H. Kataura, *Nano Lett.*, 2009, **9**, 1497–1500.
10 M. C. LeMieux, M. Roberts, S. Barman, Y. W. Jin, J. M. Kim and Z. N. Bao, *Science*, 2008, **321**, 101–104.
11 G. Y. Zhang, P. F. Qi, X. R. Wang, Y. R. Lu, X. L. Li, R. Tu, S. Bangsaruntip, D. Mann, L. Zhang and H. J. Dai, *Science*, 2006, **314**, 974–977.
12 L. Ding, A. Tselev, J. Y. Wang, D. N. Yuan, H. B. Chu, T. P. McNicholas, Y. Li and J. Liu, *Nano Lett.*, 2009, **9**, 800–805.
13 G. Hong, B. Zhang, B. H. Peng, J. Zhang, W. M. Choi, J. Y. Choi, J. M. Kim and Z. F. Liu, *J. Am. Chem. Soc.*, 2009, **131**, 14642.
14 A. R. Harutyunyan, G. G. Chen, T. M. Paronyan, E. M. Pigos, O. A. Kuznetsov, K. Hewaparakrama, S. M. Kim, D. Zakharov, E. A. Stach and G. U. Sumanasekera, *Science*, 2009, **326**, 116–120.
15 M. S. Strano, C. A. Dyke, M. L. Usrey, P. W. Barone, M. J. Allen, H. W. Shan, C. Kittrell, R. H. Hauge, J. M. Tour and R. E. Smalley, *Science*, 2003, **301**, 1519–1522.
16 L. An, Q. A. Fu, C. G. Lu and J. Liu, *J. Am. Chem. Soc.*, 2004, **126**, 10520–10521.
17 B. Yu, P. X. Hou, F. Li, B. L. Liu, C. Liu and H. M. Cheng, *Carbon*, 2010, **48**, 2941–2947.
18 K. H. An, J. S. Park, C. M. Yang, S. Y. Jeong, S. C. Lim, C. Kang, J. H. Son, M. S. Jeong and Y. H. Lee, *J. Am. Chem. Soc.*, 2005, **127**, 5196–5203.
19 M. Yudasaka, M. Zhang and S. Iijima, *Chem. Phys. Lett.*, 2003, **374**, 132–136.
20 S. Banerjee and S. S. Wong, *Nano Lett.*, 2004, **4**, 1445–1450.
21 K. Tohji, T. Goto, H. Takahashi, Y. Shinoda, N. Shimizu, B. Jeyadevan, I. Matsuoka, Y. Saito, A. Kasuya, T. Ohsuna, H. Hiraga and Y. Nishina, *Nature*, 1996, **383**, 679–679.
22 K. Hata, D. N. Futaba, K. Mizuno, T. Namai, M. Yumura and S. Iijima, *Science*, 2004, **306**, 1362–1364.
23 B. Li, X. H. Cao, X. Huang, G. Lu, Y. Z. Huang, C. F. Goh, F. Y. C. Boey and H. Zhang, *Small*, 2009, **5**, 2061–2065.
24 A. Ismach, L. Segev, E. Wachtel and E. Joselevich, *Angew. Chem., Int. Ed.*, 2004, **43**, 6140–6143.
25 C. Kocabas, S. H. Hur, A. Gaur, M. A. Meitl, M. Shim and J. A. Rogers, *Small*, 2005, **1**, 1110–1116.
26 L. Ding, D. Yuan and J. liu, *J. Am. Chem. Soc.*, 2008, **130**, 5428–5429.
27 S. J. Kang, C. Kocabas, T. Ozel, M. Shim, N. Pimparkar, M. A. Alam, S. V. Rotkin and J. A. Rogers, *Nat. Nanotechnol.*, 2007, **2**, 230–236.
28 T. Yamada, A. Maigne, M. Yudasaka, K. Mizuno, D. N. Futaba, M. Yumura, S. Iijima and K. Hata, *Nano Lett.*, 2008, **8**, 4288–4292.
29 A. Kukovecz, T. Pichler, R. Pfeiffer, C. Kramberger and H. Kuzmany, *Phys. Chem. Chem. Phys.*, 2003, **5**, 582–587.
30 M. S. Dresselhaus and P. C. Eklund, *Adv. Phys.*, 2000, **49**, 705–814.
31 A. Jorio, R. Saito, J. H. Hafner, C. M. Lieber, M. Hunter, T. McClure, G. Dresselhaus and M. S. Dresselhaus, *Phys. Rev. Lett.*, 2001, **86**, 1118–1121.
32 C. A. Wang, J. L. Zhang and C. W. Zhou, *ACS Nano*, 2010, **4**, 7123–7132.
33 Y. M. Li, S. Peng, D. Mann, J. Cao, R. Tu, K. J. Cho and H. J. Dai, *J. Phys. Chem. B*, 2005, **109**, 6968–6971.
34 B. Hu, H. Ago, N. Yoshihara and M. Tsuji, *J. Phys. Chem. C*, 2010, **114**, 3850–3856.
35 P. B. Amama, C. L. Pint, L. McJilton, S. M. Kim, E. A. Stach, P. T. Murray, R. H. Hauge and B. Maruyama, *Nano Lett.*, 2009, **9**, 44–49.
36 N. Yoshihara, H. Ago and M. Tsuji, *J. Phys. Chem. C*, 2007, **111**, 11577–11582.
37 S. Niyogi, M. A. Hamon, H. Hu, B. Zhao, P. Bhowmik, R. Sen, M. E. Itkis and R. C. Haddon, *Acc. Chem. Res.*, 2002, **35**, 1105–1113.
38 Z. F. Chen, W. Thiel and A. Hirsch, *ChemPhysChem*, 2003, **4**, 93.